Exergy Performance Analysis of a Two-Stage Dew Point Evaporative Cooler

Clara Gascó Arranz[a], Pedro Navarro Cobacho[a], Padro Martínez Martínez[a], Ana María Blanco Marigorta[b] and Javier Ruiz Ramírez[a]

[a] *Engineering Research Institute of Elche, Miguel Hernández University, Elche, Spain, cgasco@umh.es, CA*
[b] *Department of Process Engineering, University of Las Palmas de Gran Canaria, Las Palmas de Gran Canaria, Spain, anamaria.blanco@ulpgc.es*

Abstract:
This study presents a comprehensive exergy analysis of a two-stage Dew-Point Evaporative Cooler (DPEC). A 2D analytical model was developed and validated against results reported in the literature. Subsequently, to evaluate the system's sensitivity to ambient conditions and operational parameters, a parametric study was conducted in terms of exergy destruction and exergetic efficiency, analysing a total of 1600 different scenarios. Results reveal that exergy extracted from the water film during phase change and mass diffusion acts as the system's primary thermodynamic engine. Higher exergetic efficiencies are obtained in milder and drier conditions, despite the increase in exergy destruction. Regarding operational parameters, higher primary airflow rates lead to decreased efficiency, whereas no definitive trend is observed for the first-stage secondary airflow. The influence of the extraction ratio is most pronounced under dry or moderately humid conditions, where the efficiency improves with higher ratios. Under optimal conditions, an exergetic efficiency of up to 41% is achieved. Overall, this study advances beyond previous efforts in the literature by providing a second-law assessment of the two-stage DPEC, thereby complementing existing first-law analyses.

Keywords:
Exergy analysis, Evaporative cooling, Two-stage DPEC, Parametric study.

1. Introduction

Conventional mechanical vapour-compression air conditioning (AC) systems consume a substantial amount of electrical energy, contributing heavily to peak grid demands. Furthermore, these systems are responsible for significant greenhouse gas (GHG) emissions, both indirectly through fossil fuel reliant electricity generation, and directly via the leakage of high-global-warming-potential (GWP) fluorinated refrigerants [1]. Consequently, developing highly efficient, low-carbon cooling technologies is imperative to meet the ambitious targets set by the European Union (EU) for climate neutrality and a fully decarbonised building stock by 2050.

As a compelling alternative, the Maisotsenko cycle (M-cycle), also known as dew-point evaporative cooler (DPEC), provides sensible cooling beyond the traditional evaporative technologies without introducing moisture to the conditioned space [2]. In this process, a primary airstream flows through dry passages, sensibly rejecting heat to adjacent wetted channels. A fraction of this pre-cooled air is subsequently diverted into the wet channels to drive evaporation. As this secondary stream absorbs latent heat and is exhausted to the atmosphere, the primary product stream is cooled below the wet-bulb temperature, theoretically approaching the ambient dew-point.

To properly assess the true thermodynamic limits and pinpoint internal irreversibilities, researchers have increasingly applied second-law exergy analyses to evaluate DPEC performance. For instance, Lin et al. [3] conducted a detailed numerical exergy evaluation of a counter-flow DPEC, concluding that its exergy efficiency ratio exceeds unity, and thereby demonstrating a highly competitive second-law efficiency for air conditioning applications. Expanding on geometric arrangements, Kashyap et al.

[4] numerically compared various flow topologies to determine the optimal configuration yielding the higher exergy efficiency, lower specific total cost and sustainability index. The same group of authors [5] subsequently applied this framework to experimentally evaluate a dual-mode evaporative cooler, demonstrating its thermodynamic viability when switching between direct and regenerative modes across different seasons. Further broadening the empirical scope, Kousar et al. [6] experimentally assessed both cross-flow and counter-flow DPECs under a comprehensive framework that evaluated exergetic performance alongside energy, economic, and environmental indicators.

Despite these advancements, most existing DPECs rely on conventional single-stage architectures. While capable of approaching the dew point, their net cooling capacity is constrained by the high working-air ratio (typically 30–50%) required to sustain evaporation. This substantial diversion of pre-cooled air reduces the supply volume, restricting their applicability in building air-conditioning scenarios that demand high ventilation rates or face large sensible thermal loads [7].

To overcome these limitations, Chen et al. [8] recently introduced a novel two-stage DPEC that integrates four airstreams within a single compact exchanger. This architecture divides the cooling load between an initial indirect evaporative pre-cooling stage and a subsequent M-cycle stage, thereby drastically reducing the required working-air fraction. Comprehensive experimental and 3D numerical investigations [8, 9] demonstrate that this two-stage configuration preserves approximately 90% of the product airstream, achieves an Energy Efficiency Ratio (EER) of 15–17, and reaches up to 95% dew-point effectiveness. These results provide a clear basis for selecting this configuration for further exploration.

While these first-law performance evaluations establish a strong foundation, a fundamental understanding of the system's second-law thermodynamic behaviour remains unexplored. In this context, the primary objective of this work is to fill this literature gap by performing a comprehensive exergy evaluation of the two-stage DPEC. For this purpose, a 2D analytical model of the system was developed, and its results were used to formulate the exergy balance of the device. This formulation enables a detailed mapping of the exergy flows, including internal exergy destruction, as well as the determination of the overall exergetic efficiency. Furthermore, a broad parametric sweep was conducted to comprehensively evaluate the sensitivity of these exergetic performance indicators under diverse ambient conditions and operational parameters.

2. Methodology

This section includes the developed two-stage DPEC model, as well as its exergy analysis.

2.1. Two-stage DPEC model

A 2D steady-state analytical model of the two-stage DPEC was developed to simulate the heat and mass transfer processes within the system for a characteristic pair of dry-wet channels. Based on the physical prototype detailed by Chen et al. [8], this compact cross-flow exchanger consists of 141 alternating channels (71 dry and 70 wet) stacked within a single case equipped with two fans. To formulate the mathematical framework, several simplifying assumptions were adopted. Heat exchange with the external surroundings was assumed to be zero. Furthermore, due to the minimal thickness of the dividing plates, both the conductive thermal resistance of the channel walls and any transverse temperature gradients across their surfaces were neglected. The working air streams were treated as incompressible fluids, with thermophysical properties considered uniform within each local control volume. Finally, the secondary air stream was assumed to achieve complete thermodynamic saturation at the water-film interface.

As illustrated in Fig. 1, the model is formulated around a differential control volume that captures this cross-flow arrangement. Within this element, three distinct heat fluxes can be identified: the sensible heat transfer from the dry air to the water film (1), the sensible heat transfer from the water film to the secondary air stream (2), and the latent heat flux associated with the evaporation of water into the secondary air stream (3). Moreover, mass transfer takes place between the water film and the

secondary air stream on the wet channel due to evaporation (4).

$$d\dot{Q}_{s_1} = h_{c_d}(T_d - T_w)dxdy \tag{1}$$
$$d\dot{Q}_{s_2} = h_{c_s}(T_w - T_s)dxdy \tag{2}$$
$$d\dot{Q}_L = h_{Lv}d\dot{m}_w = -h_{Lv}d\dot{m}_v \tag{3}$$
$$d\dot{m}_w = -h_m\rho_v(\omega_s - \omega)dxdy \tag{4}$$

In (4) ω_s is the saturation humidity ratio of the secondary air at the water temperature. Since the flow remains laminar under all operating conditions and the channel width significantly exceeds its height, the passages are approximated as flat channels with a constant Nusselt number of $\mathrm{Nu} = 8.24$ [10]. Consequently, the convective heat transfer coefficients (h_{c_d}, h_{c_s}) are calculated using (5). The mass transfer coefficient (h_m) between the secondary air stream and the water film is represented by a function of the Lewis number and the convective heat transfer coefficient (6).

$$\mathrm{Nu} = \frac{h_c D_h}{k} \tag{5}$$
$$\mathrm{Le} = \frac{h_{c_s}}{c_{p_h} h_m \rho_v} \tag{6}$$

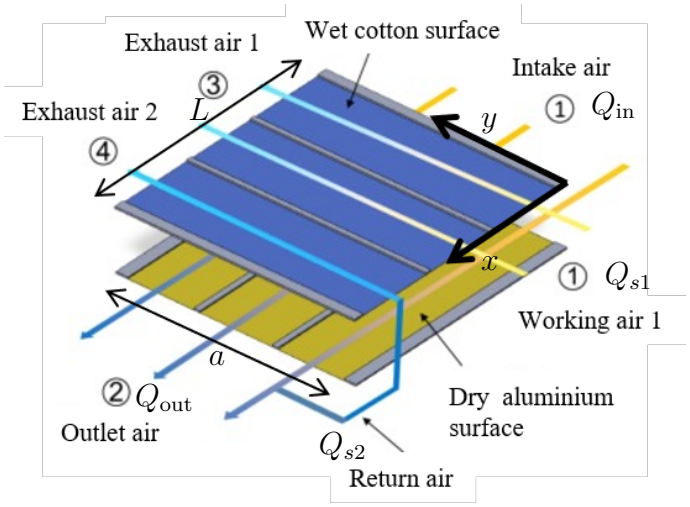

Figure 1: Air flow configuration of the two-stage DPEC, Chen et al. [8].

Assuming steady-state operation, the water film interface maintains thermal equilibrium, dictating that the net heat transfer across this boundary must be zero. By formulating an energy balance for the water film, this equilibrium is satisfied when the algebraic sum of all thermal gains and losses equals zero, as expressed in (7). Resolving this balance yields a non-linear relationship that is solely dependent on the local water temperature (T_w) where the sensible heat variation of the water film itself is denoted by $\dot{Q}_{s_c}$, detailed in (8).

$$F(T_w) = \dot{Q}_{s_a} - \dot{Q}_{s_b} + \dot{Q}_{s_c} - \dot{Q}_L = 0 \tag{7}$$
$$d\dot{Q}_{s_c} = \dot{m}_{w_{\mathrm{in}}} \cdot c_{p_w} \cdot (T_{w_{\mathrm{in}}} - T_w) \tag{8}$$

Concurrently, the principles of mass and energy conservation govern the behaviour of the interacting air streams. For the primary dry channel, the energy balance is defined by (9), which equates the drop in the air stream's enthalpy directly to its sensible heat loss. Equation (10) establishes the energy balance for the secondary air stream, attributing its enthalpy variation to the sensible heat exchange

with the water film. The mass transfer dynamics are captured by (11), illustrating how the secondary stream's humidity ratio evolves along the length of the wet channel due to evaporative processes, evaluated relative to the dry air mass flow rate. Finally, the continuity of the water film is maintained by (12), which ensures that the localised depletion of liquid water matches the vapour absorbed by the secondary air stream.

$$\dot{m}_d c_{p_{h_d}} dT_d = -d\dot{Q}_{s_a} \tag{9}$$

$$\dot{m}_s c_{p_{h_s}} dT_s = d\dot{Q}_{s_b} \tag{10}$$

$$d\omega = \frac{d\dot{m}_v}{\dot{m}_a} \tag{11}$$

$$d\dot{m}_w = -d\dot{m}_v \tag{12}$$

The primary (dry channel) and redirected (second-stage wet channel) airflow rates are related through the extraction ratio (r), defined as the ratio between the air flow through the second-stage wet channel (Q_{s2}) and the airflow entering the primary channel (Q_{in}), as given by (13).

$$r = \frac{Q_{s2}}{Q_{\text{in}}} \tag{13}$$

To resolve the system of coupled differential equations, a numerical approach is employed by discretising the channel geometry onto a 2D grid. The computational procedure advances sequentially along the fluid flow paths. For every control volume, the Newton-Raphson method is first utilised to solve (7), yielding the local interface temperature (T_w). Upon reaching thermal equilibrium, the nodal outlet conditions, including air temperature, humidity, and water mass flow rate, are calculated and forwarded as inlet parameters for the adjacent downstream node. Nevertheless, an iterative feedback loop is introduced to address the system's regenerative configuration, as the initial boundary conditions for the second-stage wet channel depend on the primary air outlet. The solver continuously evaluates the entire domain until the discrepancy between the primary air outlet temperature and the secondary inlet temperature falls within a strict convergence tolerance. Ultimately, the simulation provides comprehensive spatial profiles for the temperature and humidity of all interacting air streams, as well as the thermal and mass characteristics of the water film.
Furthermore, the power consumed by the fans, $\dot{W}_{\text{fan}}$, is determined via (14). It relies on the volumetric air flow rate, Q, the system's pressure drop, Δp, and an assumed constant fan efficiency of $\eta_{\text{fan}} = 0.36$. Within this expression, Δp is derived from an empirical correlation linking the pressure drop to the air flow rate from Chen et al. [8].

$$\dot{W}_{\text{fan}} = \frac{Q \cdot \Delta p}{\eta_{\text{fan}}} \tag{14}$$

2.2. Exergy analysis

Exergy represents the maximum theoretical useful work that can be extracted from a system as it is brought into thermodynamic equilibrium with its surrounding environment [11]. Consequently, the calculated exergy of any material stream is inherently tied to the precise specification of this reference environment. Upon reaching this state of complete balance, the system is said to be at the dead state. According to Wepfer et al. [12], the fundamental dead state is attained when all constituents of the system achieve total thermal, mechanical, and chemical equilibrium with the stable components of the surroundings, meaning the system's temperature, pressure, and chemical potentials become indistinguishable from the environment conditions. Since a universally standardised reference does not exist, the appropriate dead state parameters must be adapted to the specific process and local environment under investigation. In this study, the reference pressure is fixed at the standard barometric value of $p_0 = 101.325$ kPa. The ambient dry-bulb temperature is adopted as the dead state temperature (T_0).

Finally, although a definitive consensus regarding dead state humidity remains absent in the literature, the outdoor ambient moisture level is selected as the reference value [12]. This choice aligns with the core definition of exergy, which dictates full system equilibration with its surroundings.
Once the analytical model is solved, the local thermodynamic conditions of the interacting air streams and the water film are determined at every coordinate within the exchanger. Consequently, dependent energetic parameters, such as enthalpy, can be readily deduced. The total available work potential transported by a fluid stream is characterised as its flow exergy [13]. For the purposes of this investigation, the working fluids comprise humid air and liquid water, and their respective specific flow exergies are calculated according to (15) and (16). In these equations $\tilde{\omega}$ is the absolute humidity in a molar basis ($\tilde{\omega} = 1.608\omega$). Both formulations encompass the physical and chemical exergy components. For the humid air stream, the first two terms denote the physical exergy, while the final term defines the chemical exergy. Conversely, the liquid water formulation integrates both contributions into a single expression. This unified approach reflects that, at the ultimate dead state, the liquid water will have evaporated, thereby becoming a constituent of an ideal mixture, which is the reference ambient wet air.

$$e_{ha} = c_{ha}T_0\left(\frac{T}{T_0} - 1 - \ln\left(\frac{T}{T_0}\right)\right) + (1+\tilde{\omega})R_aT_0\ln\left(\frac{p}{p_0}\right) + \\ + R_aT_0\left[(1+\tilde{\omega})\ln\left(\frac{1+\tilde{\omega}_0}{1+\tilde{\omega}}\right) + \tilde{\omega}\ln\left(\frac{\tilde{\omega}}{\tilde{\omega}_0}\right)\right] \tag{15}$$

$$e_w = h_w(T,p) - h_0(T_0,p_{w,0}) - T_0\left[s_w(T,p) - s_0(T_0,p_{w,0})\right] \tag{16}$$

The exergy balance is formulated for the overall two-stage DPEC control volume. Within this balance, the exergy of the product ($\dot{E}_P$) represents all exergy increments that align with the functional objective of the device. Conversely, the exergy of the fuel ($\dot{E}_F$) aggregates the exergy of the supplied energy streams and internal exergy reductions expended to drive the process [14]. For the evaluated two-stage DPEC, the core objective is to cool the primary air stream. Because this thermal exchange occurs at temperatures below the dead state (T_0), exergy flows in the opposite direction to heat transfer [11]. Consequently, removing heat from the primary air results in an increase in its exergy, constituting the system's product exergy, as defined in (17). The driving exergy necessary to achieve this cooling is drawn from the water film, the first secondary air stream, and the mechanical power supplied by the fans ($\dot{W}_{\text{fan}}$), as expressed in (18). Notably, because the second wet channel is fed by recirculated primary air, its intake is treated as an internal flow within the control volume rather than an external supply. Any unutilised exergy discharged to the surroundings by the exhaust secondary streams is classified as exergy loss, $\dot{E}_L$ (19). Ultimately, the exergy destruction ($\dot{E}_D$), arising from internal irreversibilities is quantified by closing the overall balance in (20).

$$\dot{E}_P = \Delta\dot{E}_d = \dot{m}_{d,2}\cdot e_{d,2} - \dot{m}_{d,1}\cdot e_{d,1} \tag{17}$$

$$\dot{E}_F = \dot{E}_{s1,1} + \Delta\dot{E}_w + \dot{W}_{\text{fan}} = \dot{m}_{s1,1}\cdot e_{s1,1} + (\dot{m}_{w,1}\cdot e_{w,1} - \dot{m}_{w,2}\cdot e_{w,2}) + \dot{W}_{\text{fan}} \tag{18}$$

$$\dot{E}_L = \dot{E}_{s1,2} + \dot{E}_{s2,2} = \dot{m}_{s1,2}\cdot e_{s1,2} - \dot{m}_{s2,2}\cdot e_{s2,2} \tag{19}$$

$$\dot{E}_D = \dot{E}_F - \dot{E}_P - \dot{E}_L \tag{20}$$

The exergetic efficiency quantifies the actual thermodynamic effectiveness of a process. It is calculated as the ratio of the product exergy to the fuel exergy [11], as expressed in (21).

$$\varepsilon = \frac{\dot{E}_P}{\dot{E}_F} \tag{21}$$

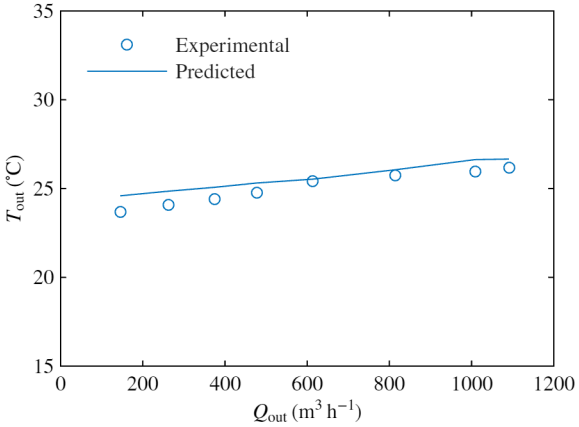

Figure 2: Comparison between experimental and predicted results with Chen et al. [8]

3. Results and discussion

3.1. Experimental validation

To verify the accuracy of the developed two-stage DPEC model, its predictions are compared with two distinct sets of results available in the literature. The first evaluation relies on the experimental findings published by Chen et al. [8], who physically characterised a prototype of the system. As depicted in Fig. 2, the model outputs demonstrate strong agreement with the measured data, registering an average discrepancy of less than 2.3%.

Following this experimental validation, a further numerical cross-verification is performed using the comprehensive 3D CFD simulations previously published by the same research group [9]. Fig. 3 displays the contour plots for the primary air temperature, alongside the secondary air temperature and humidity, obtained from both modelling approaches. From a qualitative perspective, the current 2D model accurately captures the spatial distributions and thermal gradients evident in the 3D reference case. This visual agreement is corroborated by quantitative metrics at the device outlets, where the maximum deviations across all evaluated parameters (temperature and humidity) are kept below 2%.

3.2. Exergy flow analysis

To visualise the thermodynamic behaviour of the two-stage DPEC, Fig. 4 presents the Grassmann diagram for a representative operational point ($T_{\text{amb}} = 30$°C, $\phi_{\text{amb}} = 0.35$, $Q_{\text{in}} = 250$ m^3 h^{-1}, $Q_{s1} = 100$ m^3 h^{-1}, $r = 0.1$). This diagram effectively maps the magnitude and distribution of exergy from its supply to its final conversion, destruction, or loss, providing a clear anatomical breakdown of the system's irreversibilities.

On the input side, the total fuel exergy ($\dot{E}_F$) driving the system amounts to 63.7 W, which is composed of two distinct streams. The majority of this available exergy, representing 98% (62.6 W), originates from the exergy extracted from the water film ($\Delta\dot{E}_w$). This highlights that the phase change and the mass transfer of water diffusing into the dry airstream act as the primary thermodynamic engine of the device. The remaining 2% (1.1 W) is the mechanical power supplied by the fans ($\dot{W}_{\text{fan}}$) required to force the airflows through the narrow channels. Tracing the flow to the right side of the diagram reveals how this supplied fuel is distributed. The useful product exergy ($\dot{E}_P$), which corresponds to the absolute sensible cooling achieved in the delivered primary airstream, accounts for only 24% (15.3 W) of the total input. This distribution reflects the inherently low overall exergetic efficiency characteristic of evaporative cooling technologies. The vast majority of the supplied exergy is penalised through losses and internal destruction. The exergy loss ($\dot{E}_L$) constitutes the largest single fraction at 43% (27.7 W). This represents the thermodynamic potential carried away by the saturated secondary exhaust streams, which are discharged directly into the environment and remain unutilised. Finally, the internal exergy destruction ($\dot{E}_D$) consumes 33% (20.8 W) of the total fuel. This substantial

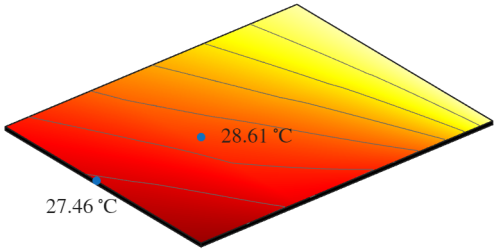

(a) Predicted primary air temperature distribution.

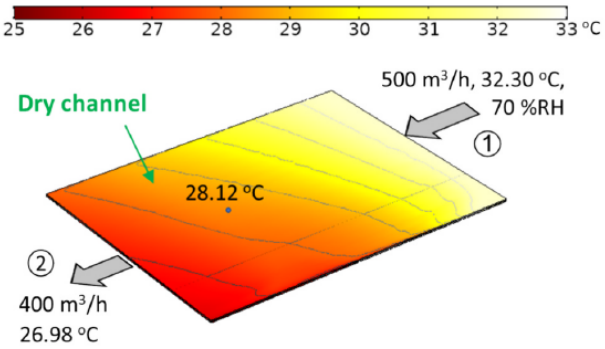

(b) Primary air temperature distribution, [9].

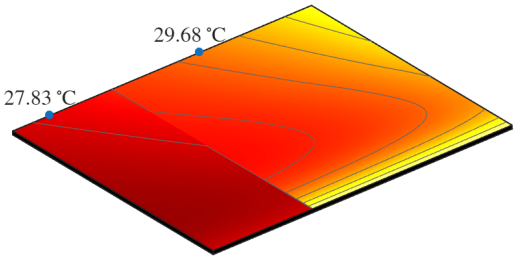

(c) Predicted secondary air temperature distribution.

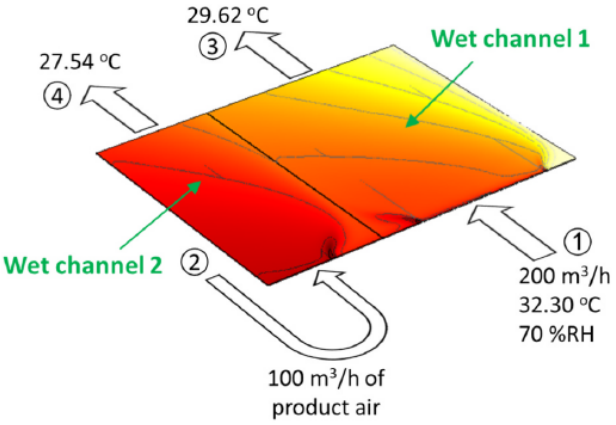

(d) Secondary air temperature distribution, [9].

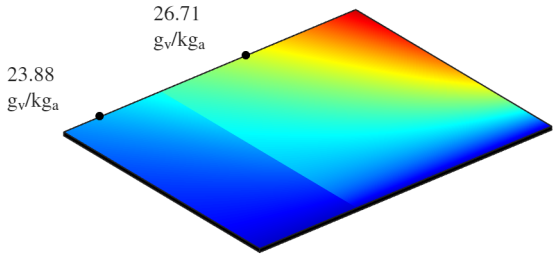

(e) Predicted secondary air humidity distribution.

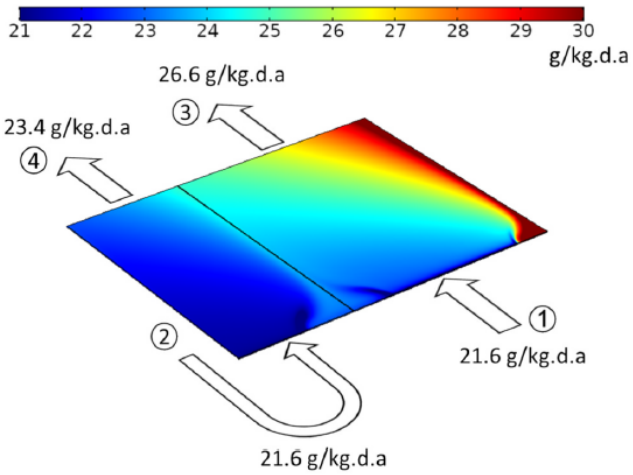

(f) Secondary air humidity distribution, [9].

Figure 3: Temperature and humidity distribution in two-stage DPEC comparison between developed model and [9] predicted results.

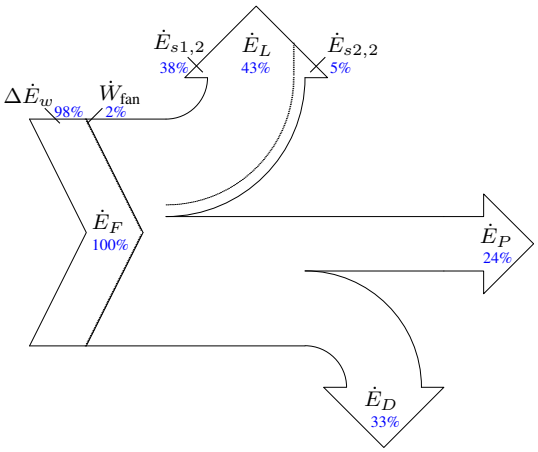

Figure 4: Exergy flow diagram for $T_{\text{amb}} = 30$ºC, $\phi_{\text{amb}} = 0.35$, $Q_{\text{in}} = 250$ m^3 h^{-1}, $Q_{s1} = 100$ m^3 h^{-1}, $r = 0.1$.

Table 1: Variables and levels considered in the parametric study.

T_{amb} (ºC)	ϕ_{amb} $(-)$	Q_{in} (m^3 h^{-1})	Q_{s1} (m^3 h^{-1})	r (-)
20	0.15	250	50	0.05
25	0.35	500	100	0.1
30	0.55	750	200	0.15
35	0.75	1000	300	0.2
40	0.95			

destruction is driven by the inherent irreversibilities occurring within the core, such as heat transfer across finite temperature differences between adjacent streams, and the chemical irreversibilities of water evaporating into the air.

3.3. Parametric study

While the preceding exergy flow analysis provides a fundamental understanding of the system's irreversibilities at a single representative state, these thermodynamic distributions are highly sensitive to external variations. Consequently, a parametric study was conducted to comprehensively evaluate the thermodynamic behaviour of the proposed two-stage DPEC under a wide range of boundary conditions. The investigation focuses on two Key Performance Indicators (KPIs) based on rigorous exergetic criteria: the exergy destruction ($\dot{E}_D$) and the overall exergetic efficiency (ε). Table 1 details the variables and their corresponding levels considered in this parametric study, yielding a total of 1600 simulated scenarios. The parametric sweep encompasses both environmental and operational variables. First ones are defined by the ambient temperature (T_{amb}) and relative humidity (ϕ_{amb}). The operational parameters evaluated are the primary inlet volumetric airflow rate (Q_{in}), the volumetric airflow rate supplied to the first-stage secondary airstream (Q_{s1}), and the extraction airflow ratio (r). As an evaporative cooling technology, the performance of the two-stage DPEC is strongly dependent on ambient conditions. Larger temperature drops between the inlet and outlet primary air are obtained under high ambient temperatures and low humidity levels, owing to the greater wet-bulb depression that significantly enhances the driving force for water evaporation. Fig. 5(a) depicts the influence of these environmental variables on both KPIs (exergy destruction and exergetic efficiency), evaluated for a reference case ($Q_{\text{in}} = 500$ m^3 h^{-1}, $Q_{s1} = 100$ m^3 h^{-1}, $r = 0.1$). Under hotter and drier conditions, the intensified evaporation rate extracts more exergy from the water film ($\Delta\dot{E}_w$), which directly results in a higher total fuel exergy ($\dot{E}_F$). Correspondingly, this enhanced evaporative effect yields a larger product exergy ($\dot{E}_P$) stemming from the superior cooling achieved in the primary stream. Regarding the exergy loss and the exergy destruction, both metrics exhibit identical qualitative

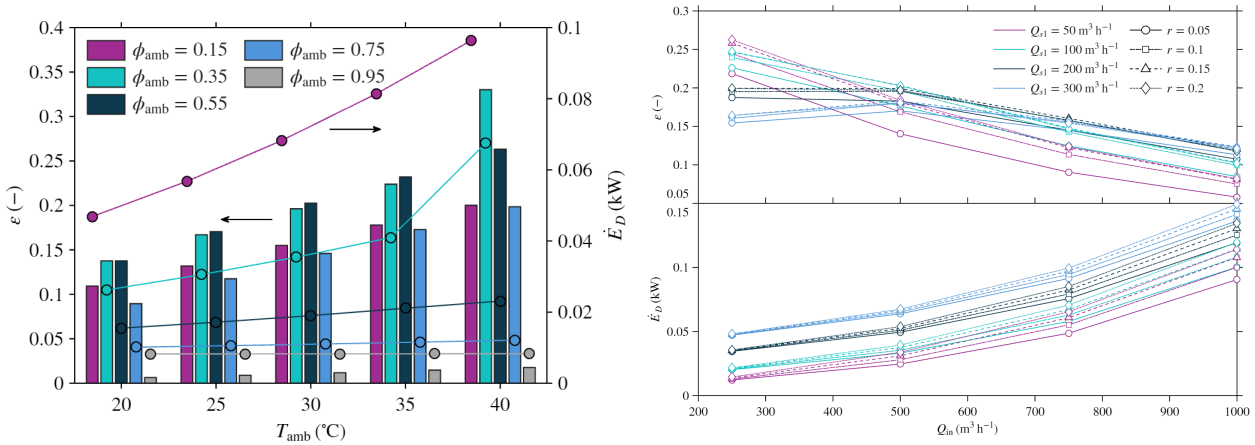

(a) Effect of T_{amb}, ϕ_{amb} (Q_{in} = 500 m^3 h^{-1}, Q_{s1} = 100 m^3 h^{-1}, $r = 0.1$).

(b) Effect of Q_{in}, Q_{s1}, r ($T_{amb} = 30$ºC, $\phi_{amb} = 0.35$).

Figure 5: Influence of: (a) ambient conditions; (b) operational variables on KPIs ($\dot{E}_D$, ε).

behaviour, intensifying at elevated temperatures and reduced humidities, due to the larger thermal and concentration gradients driving the heat and mass transfer, which naturally generate greater internal irreversibilities and exhaust losses. Ultimately, because the relative surge in product exergy outpaces the growth of the consumed fuel, the overall exergetic efficiency increases with ambient temperature. Nevertheless, the balance between these exergy terms exhibits a distinct, non-linear dependence on ambient humidity, with the highest exergetic efficiency achieved at moderate relative humidity values, followed by a steep decline under highly humid conditions where the evaporative cooling potential becomes negligible.

Fig. 5(b) illustrates the behaviour of both exergy destruction and exergetic efficiency in response to the operational parameters, evaluated under a reference ambient condition ($T_{amb} = 30$ºC, $\phi_{amb} = 35\%$). Addressing the primary inlet airflow (Q_{in}), driving a larger volume of air through the channels can increase the absolute sensible cooling even with decreased temperature drops between inlet and outlet, but also inherently elevates fluid velocities and internal friction. This directly causes a surge in the required mechanical fan power, significantly increasing the fuel exergy. Furthermore, the proportional increase in the redirected evaporative airstream ($r \cdot Q_{in}$) intensifies mass transfer, which, coupled with the heightened fluid friction, rises the exergy destruction ($\dot{E}_D$). Because this escalation in consumed fuel and internal destruction outweighs the marginal gains in absolute sensible cooling (product exergy, $\dot{E}_P$), the overall exergetic efficiency decreases as Q_{in} grows. Conversely, the first-stage secondary airflow rate (Q_{s1}) actively drives the evaporative cooling process in the first stage. Therefore, increasing Q_{s1} enhances the local heat and mass transfer rates, which leads to higher product exergy ($\dot{E}_P$) by improving the primary stream cooling. However, this also inherently increases the generated irreversibilities ($\dot{E}_D$) and the required fuel exergy. As a result of these opposing effects, the exergetic efficiency does not follow a specific trend. Finally, the extraction ratio (r) dictates the fraction of pre-cooled primary air redirected to feed the second evaporative stage. Thus, increasing r significantly boosts the evaporative potential of this second stage, leading to a larger temperature drops across the primary stream. However, this inevitably causes a reduction in the final product mass flow rate. The total cooling capacity is therefore determined by the balance of these two competing factors. Under the moderate ambient humidity of the reference case, the enhanced temperature reduction dominates, yielding a substantial overall gain in product exergy ($\dot{E}_P$). Concurrently, both the fuel exergy and exergy destruction also increase due to the intensified mass transfer and the added fluid friction associated with driving a larger air fraction through the second-stage wet channel. Nevertheless, these penalties are effectively counterbalanced by the growth in the system's cooling output. As a result, the exergetic efficiency exhibits an upward trend with higher extraction ratios.

Extending the analysis to the complete set of simulated cases, Table 2 summarises the global in-

Table 2: Summary of the parametric study. ↑: increase; ↓: decrease; −: no effect; ∼: medium value/similar.

Increasing	$\dot{E}_F$	$\dot{E}_P$	$\dot{E}_L$	$\dot{E}_D$	ε
T_{amb}	↑	↑	↑	↑	↑
ϕ_{amb}	↓	↓	↓	↓	↑↓
$\dot{Q}_{\text{in}}$	↑	↑↓	↑	↑	↓
r if ↓∼ ϕ_{amb}	↑	↑	↑	↑	↑
r if ↑ ϕ_{amb}	−	∼↓	↑	−	−
$\dot{Q}_{s1}$	↑	↑	↑	↑	↑ ($\dot{Q}_{\text{in}} = 750 - 1000$ m^3 h^{-1}) ↑↓ ($\dot{Q}_{\text{in}} = 250 - 500$ m^3 h^{-1})

fluence of each parameter on the exergetic balance components and the main KPIs. While detailed results were previously discussed for a reference scenario, these qualitative trends remain largely consistent across the full parametric domain. The primary exception arises under high ambient humidity, where the evaporative cooling potential is severely limited. Thus, variations in operational parameters, such as the extraction ratio (r), yield a negligible impact on the system's performance, as the mass transfer mechanism is almost entirely suppressed. A notable conclusion from this analysis is that the overall exergetic efficiency of the two-stage DPEC remains inherently low regardless of the operating conditions. This is fundamentally due to the substantial internal irreversibilities generated by heat transfer and mass diffusion, the significant exhaust exergy rejected to the atmosphere ($\dot{E}_L$), and the intrinsically low specific exergy of the sensibly cooled primary airstream. The optimal thermodynamic configuration, yielding the highest exergetic efficiency ($\varepsilon = 41\%$), is obtained at $T_{\text{amb}} = 40$°C and $\phi_{\text{amb}} = 35\%$ with low-throughput operational parameters ($Q_{\text{in}} = 250$ m^3 h^{-1}, $Q_{s1} = 50$ m^3 h^{-1}, $r = 0.2$). Under these ideal conditions, the exergy destruction amounts to $\dot{E}_D = 27.3$ W. Conversely, the worst-case scenario ($\varepsilon = 0.033\%$) is achieved under heavily saturated, low-temperature ambient conditions ($T_{\text{amb}} = 20$ °C, $\phi_{\text{amb}} = 95\%$) combined with high primary airflow settings ($Q_{\text{in}} = 1000$ m^3 h^{-1}, $Q_{s1} = 50$ m^3 h^{-1}, $r = 0.05$). In this highly constrained operational state, the required mechanical power dominates the exergy balance, and the exergy destruction surges to 64.6 W. Despite these seemingly low absolute values, this exergetic efficiency range is highly consistent with those of other dew-point evaporative cooling technologies reported in the literature [3, 6].

4. Conclusion

This study presented a comprehensive second-law assessment of the novel two-stage DPEC. To identify the system's internal irreversibilities and evaluate its sensitivity to diverse environmental and operational conditions, an exergy analysis and a broad parametric sweep were conducted using a 2D analytical model. From this investigation, the following main conclusions can be drawn:

- Exergy extracted from the water film during phase change and mass diffusion acts as the primary thermodynamic engine of the device, while the mechanical power supplied by the fans constitutes a negligible fraction of the overall fuel exergy.
- Drier and hotter conditions provide a greater thermodynamic potential for mass transfer, which increases all exergy flows: available fuel exergy, product exergy, exergy losses, and exergy destruction. As a result, the overall exergetic efficiency increases with ambient temperature, while its maximum value is achieved under moderate humidity levels.
- Higher primary airflow rates increase the required mechanical fan power, leading to a surge in overall fuel exergy. However, this additional input predominantly translates into higher internal exergy destruction and exhaust losses, thereby decreasing the overall exergetic efficiency. Regarding the first-stage secondary airflow, higher rates increase exergy destruction, although no definitive trend is observed concerning the overall exergetic efficiency. The influence of the

extraction ratio is most pronounced under dry or moderately humid conditions. In these environments, higher extraction ratios successfully improve exergetic efficiency despite the exergy destruction also rises.

Overall, the results indicate that the potential of the novel two-stage DPEC as a sustainable and highly effective alternative for building air-conditioning is substantial in hot and dry climates, where exergetic efficiencies up to 41% can be achieved with optimised operational parameters. By maintaining competitive second-law performance while successfully overcoming the capacity constraints of conventional single-stage systems, this dual-stage architecture proves to be a thermodynamically robust solution for next-generation cooling.

Acknowledgments

This publication is part of the R&D project PID2022-140796NA-I00 funded by MICIU/AEI/10.13039/501100011 and by "FEDER A way of making Europe".

Nomenclature

c_p	specific heat, J kg^{-1} K^{-1}
D_h	hydraulic diameter, m
e	exergy flow, J kg^{-1}
$\dot{E}_D$	exergy destruction, W
$\dot{E}_F$	exergy fuel, W
$\dot{E}_L$	exergy loss, W
$\dot{E}_P$	product exergy, W
h	specific enthalpy, J kg^{-1}
h_c	convection heat transfer coefficient, W m^{-2} K^{-1}
h_m	mass transfer coefficient, $\mathrm{m\ s}^{-1}$
Le	Lewis number
$\dot{m}$	mass flow rate, $\mathrm{kg\ s}^{-1}$
Nu	Nusselt number
Δp	pressure drop, Pa
Q	volumetric flow rate, $\mathrm{m}^3\ \mathrm{s}^{-1}$
$\dot{Q}_L$	latent heat transfer rate, W
$\dot{Q}_s$	sensible heat transfer rate, W
r	extraction rate
R_a	dry air specific gas constant, J kg^{-1} K^{-1}
s	specific entropy, J kg^{-1} K^{-1}
T	temperature, $^\circ\mathrm{C}$
$\dot{W}_{\mathrm{fan}}$	fan power consumption, W

Greek symbols

η	fan efficiency
ϕ	relative humidity
ω	absolute humidity, $\mathrm{kg\ kg}^{-1}$
ρ	density, $\mathrm{kg\ m}^{-3}$
ε	exergetic efficiency

Subscripts and superscripts

amb	ambient conditions
d	primary air stream
ha	humid air
$s1$	first-stage secondary airflow
$s2$	second-stage secondary airflow
v	water vapour
w	water
0	dead state

References

[1] Santamouris M., Kolokotsa D., *On the impact of urban overheating and extreme climatic conditions on housing, energy, comfort and environmental quality of vulnerable population in Europe*. *Energy and Buildings* 2015;98. Renewable Energy Sources and Healthy Buildings:125–133.

[2] Sadighi Dizaji H., Hu E. J., Chen L., *A comprehensive review of the Maisotsenko-cycle based air conditioning systems*. *Energy* 2018;156:725–749.

[3] Lin J., Bui D. T., Wang R., Chua K. J., *On the exergy analysis of the counter-flow dew point evaporative cooler*. *Energy* 2018;165:958–971.

[4] Kashyap S., Sarkar J., Kumar A., *Exergy, economic, environmental and sustainability analyses of possible regenerative evaporative cooling device topologies*. *Building and Environment* 2020;180:107033.

[5] Kashyap S., Sarkar J., Kumar A., *Experimental exergy, economic and sustainability analyses of the dual-mode evaporative cooler*. *International Journal of Refrigeration* 2022;135:121–130.

[6] Kousar R., Ali M., Amjad M. K., Ahmad W., *Energy, Exergy, Economic, Environmental (4Es) comparative performance evaluation of dewpoint evaporative cooler configurations*. *Journal of Building Engineering* 2022;45:103466.

[7] Jia L., Liu J., Wang C., Cao X., Zhang Z., *Study of the thermal performance of a novel dew point evaporative cooler*. *Applied Thermal Engineering* 2019;160:114069.

[8] Chen Z. et al., *A first-of-its-kind two-stage dew-point evaporative cooler with high energy efficiency and compact design*. *Energy Conversion and Management* 2025;341:120090.

[9] Chen Z. et al., *Energy-efficient cooling beyond M–cycle: development and evaluation of a two-stage dew-point evaporative cooler*. *Applied Thermal Engineering* 2025;280:128031.

[10] Kandlikar S. G., *Chapter 3 - Single-phase liquid flow in minichannels and microchannels*. In: Kandlikar S. G., Garimella S., Li D., Colin S., King M. R., editors. Heat Transfer and Fluid Flow in Minichannels and Microchannels. Oxford: Elsevier Science Ltd. 2006. p. 87–136.

[11] Bejan A., Tsatsaronis G., Moran M. J., *Thermal design and optimization*. John Wiley & Sons, 1995.

[12] Wepfer W. J., Gaggioli R., Obert E. F., *PROPER EVALUATION OF AVAILABLE ENERGY FOR HVAC*. In: ASHRAE Trans; 1979:214–230.

[13] Bejan A., *Advanced engineering thermodynamics*. John Wiley & Sons, 2016.

[14] Lazzaretto A., Tsatsaronis G., *SPECO: A systematic and general methodology for calculating efficiencies and costs in thermal systems*. *Energy* 2006;31(8):1257–1289.